Finding a mononuclear cobalt(III)-peroxo complex with 1,4,7,10-tetraazacyclododecane, an intermediate for dioxygen reduction

Yan Zhang [ab], Xiao-Fang Qi [a], Can-Hao Li [a], Shu-Zhong Zhan*[a]

a Chemistry & Chemical Engineering, South China University of Technology, Guangzhou 510640, China

b City College of Dongguan University of Technology, Dongguan 523419, China

Supplementary Materials

Table of context

7	**Fig. S5.** Infrared spectra of the reaction solution of $[Co(L)(Cl)_2]Cl$ **1** (0.10 mM) generated upon constant potential electrolysis experiment with $^{16}O_2$ or $^{18}O_2$ in acetonitrile-water under at -0.2 V.
8	**Fig. S6.** UV−vis absorption spectrum of complex **1** (0.02 mM) in acetonitrile under -0.20 V with H^+ (1.0 mM) at room temperature.
9	**Fig. S7.** Infrared spectrum of $[Co(L)(\mu\text{-}OH)(\mu\text{-}OO)Co(L)]Cl_3$ **2**.
10	**Fig. S8.** Raman spectrum of $[Co(L)(\mu\text{-}OH)(\mu\text{-}OO)Co(L)]Cl_3$ **2**.
11	**Fig. S9.** Rotating ring-disk electrode (RRDE) measurement for O_2 reduction at the glassy carbon (GC) disk electrode loaded with $[Co(L)(Cl)_2]Cl$ **1** in an O_2-saturated 0.1 M KOH solution at various rotation rates. Conditions: work electrode, GC disk electrode; counter electrode, Pt ring electrode, 25 °C.
12	**Fig. S10.** RRDE measurement for O_2 reduction of the ring current loaded with $[Co(L)(Cl)_2]Cl$ **1** in an O_2-saturated 0.1 M KOH solution at various rotation rates. Conditions: work electrode, GC disk electrode; counter electrode, Pt ring electrode, 25 °C.
13	**Fig. S11.** RRDE measurement for O_2 reduction at the GC disk electrode loaded with $[Co(L)(Cl)_2]Cl$ **1** in an O_2-saturated with 1600 rpm at various KOH concentrations. Conditions: work electrode, GC disk electrode; counter electrode, Pt ring electrode, 25 °C.
14	**Fig. S12.** RRDE measurement for O_2 reduction of the ring current loaded with $[Co(L)(Cl)_2]Cl$ **1** in an O_2-saturated with 1600 rpm at various KOH concentrations. Conditions: work electrode, GC disk electrode; counter electrode, Pt ring electrode, 25 °C.
15	**Fig. S13.** RRDE measurement for O_2 reduction at the GC disk electrode loaded with $[Co(L)(Cl)_2]Cl$ **1** in a N_2-saturated and in an O_2-saturated 0.1 M KOH solution with 1600 rpm. Conditions: work electrode, GC disk electrode; counter electrode, Pt ring electrode, 25 °C.

16	**Fig. S14.** RRDE measurement for O_2 reduction of the ring current loaded with $[Co(L)(Cl)_2]Cl$ **1** in a N_2-saturated and in an O_2-saturated 0.1 M KOH solution with 1600 rpm. Conditions: work electrode, GC disk electrode; counter electrode, Pt ring electrode, 25 °C.
17	**Fig. S15.** The selectivity ($\%H_2O_2$) as a function of the disk potential with varying rotation rates, in 0.1 M KOH solution.
18	**Fig. S16.** The selectivity ($\%H_2O_2$) as a function of the disk potential with different KOH concentrations at 1600 rpm.

Physical measurements

A Perkin-Elmer analyzer model 240 was used to do elemental analyses for C, H, and N. A Hitachi U-3010 spectrophotometer was used to measure UV-vis spectra of the samples. IR spectra were obtained as KBr pellets on a Bruker 1600 FT-IR spectrometer from 4000 to 400 cm^{-1}. Electron paramagnetic resonance (EPR) spectra of the cobalt complexes were taken on a Bruker Elexsys II E500 EPR spectrometer. Electrochemical measurements and analysis were conducted by using a CHI-660E electrochemical analyzer.

Determination for crystal structures of the cobalt complexes

Measurement and analyses for the structures of the cobalt complexes were conducted on a Bruker Smart Apex II DUO area detector employing graphite monochromated Mo-Kα radiation (λ = 0.71073 Å). All empirical absorption corrections were conducted on the SADABS program. [1] Direct method was used to analyze the structures of the cobalt complexes and the corresponding non-hydrogen

atoms were refined with the XL refinement package. [2] All calculations were carried out on a ShelXS structure solution program. [3] Non-hydrogen atoms were refined anisotropically, while hydrogen atoms on carbon atoms were generated geometrically and refined isotropically.

1 G. M. Sheldrick, SADABS, Program for Empirical Absorption Correction of Area Detector Data, University of Götingen, Götingen, Germany, 1996.

2 O. V. Dolomanov, L. J. Bourhis, R. J. Gildea, J. A. K. Howard and H. Puschmann, OLEX2: a complete structure solution, refinement and analysis program. *J. Appl. Cryst*., 2009, **42**, 339-341.

3 G. M. Sheldrick, Crystal structure refinement with SHELXL. *Acta Cryst*., 2015, **C17**, 3-8.

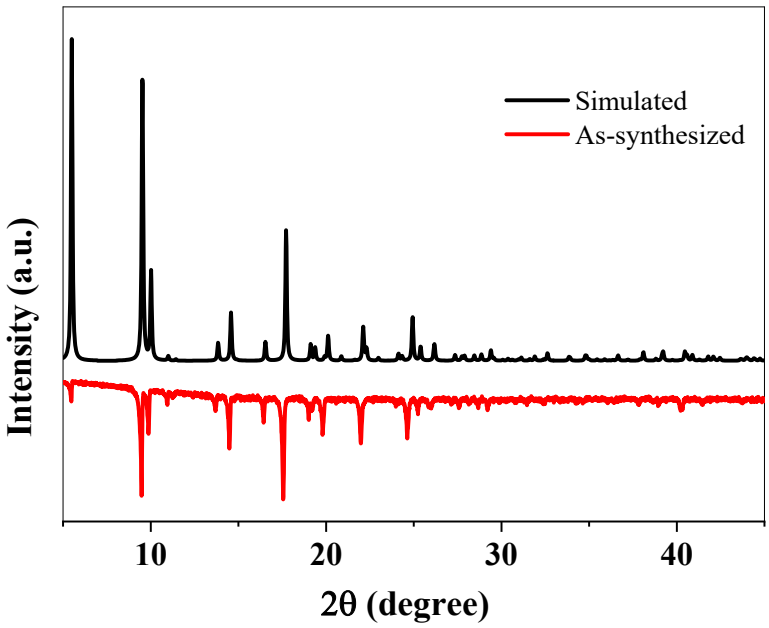

Fig. S1. Powder X-ray diffraction of $[Co(L)(Cl)_2]Cl$ **1**. As-synthesized (up); Simulated (down).

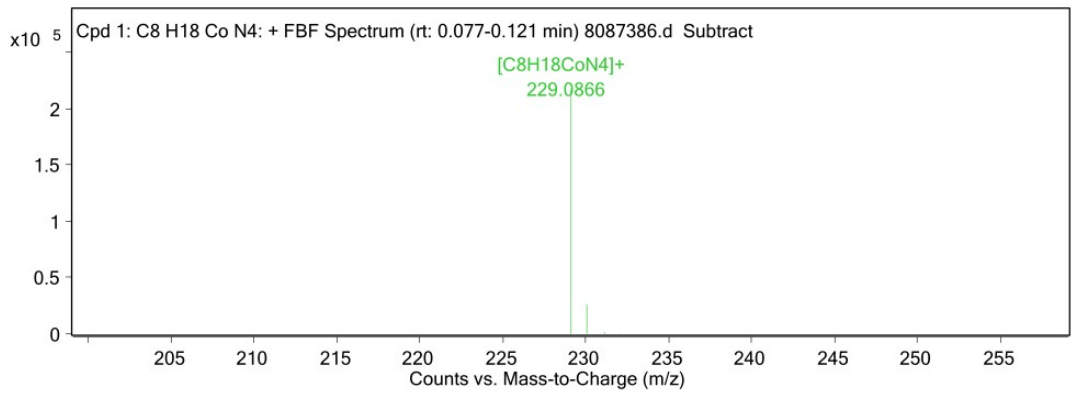

Fig. S2. ESI-MS of $[Co(L)(Cl)_2]Cl$ **1** in CH_3CN.

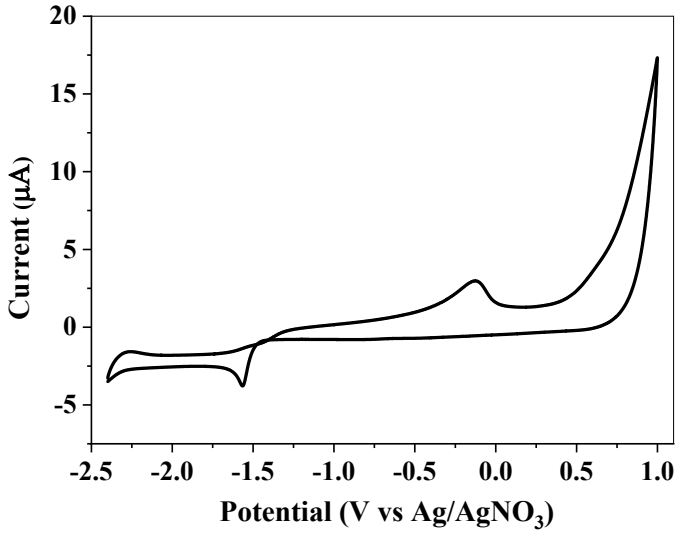

Fig. S3. (a) CV of 6.5 mM $CoCl_2$ in CH_3CN. Conditions: 0.10 M [*n*-Bu_4N]ClO_4 as supporting electrolyte, scan rate: 100 mV/s, glassy carbon working electrode (1 mm diameter), Pt counter electrode, $Ag/AgNO_3$ reference electrode.

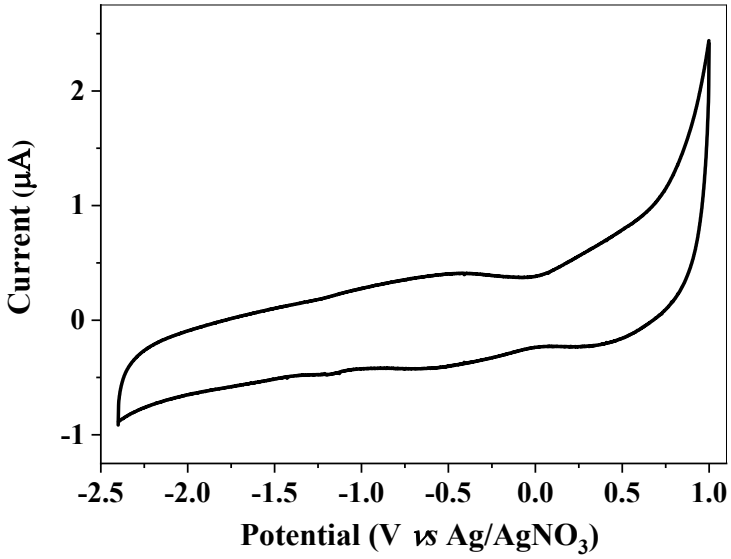

Fig. S4. CV of the ligand (6.5 mM) in CH_3CN. Conditions: 0.10 M [*n*-Bu_4N]ClO_4 as supporting electrolyte, scan rate: 100 mV/s, glassy carbon working electrode (1 mm diameter), Pt counter electrode, $Ag/AgNO_3$ reference electrode.

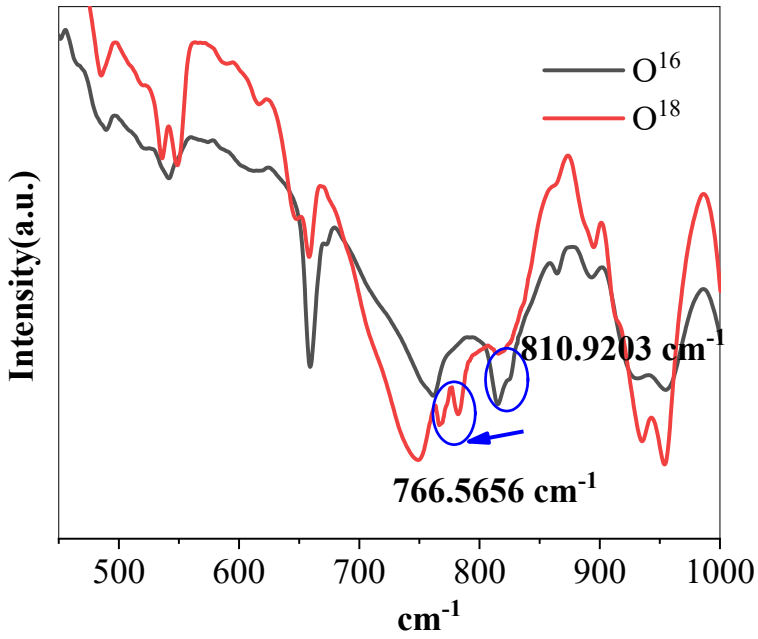

Fig. S5. Infrared spectra of the reaction solution of $[Co(L)(Cl)_2]Cl$ **1** (0.10 mM) generated upon constant potential electrolysis experiment with $^{16}O_2$ or $^{18}O_2$ in acetonitrile-water under at -0.2 V.

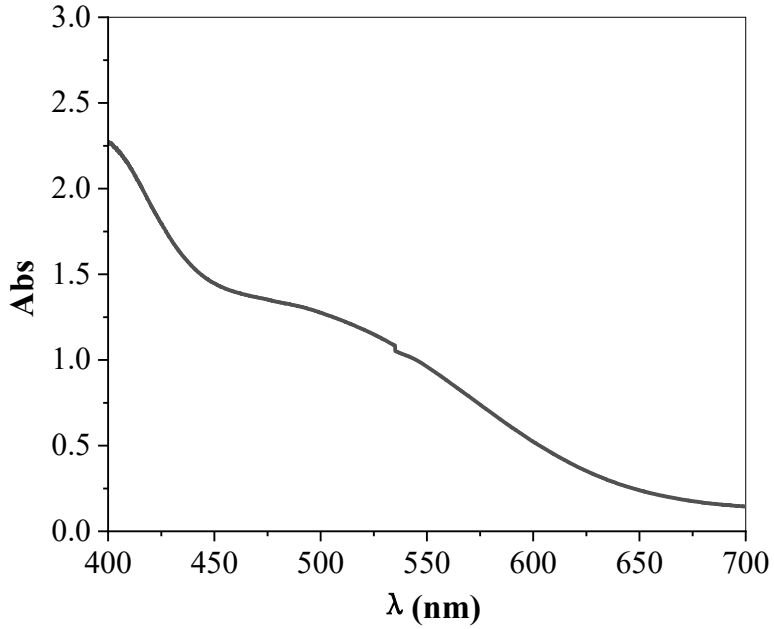

Fig. S6. UV−vis absorption spectrum of complex **1** (0.02 mM) in acetonitrile under -0.20 V with H^+ (1.0 mM) at room temperature.

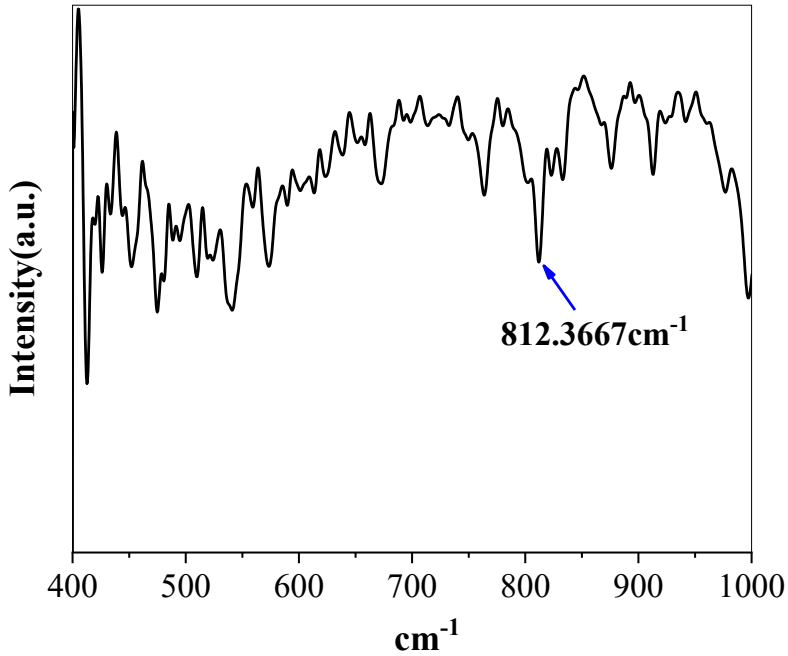

Fig. S7. Infrared spectrum of [Co(L)(μ-OH)(μ-OO)Co(L)]Cl_3 **2**.

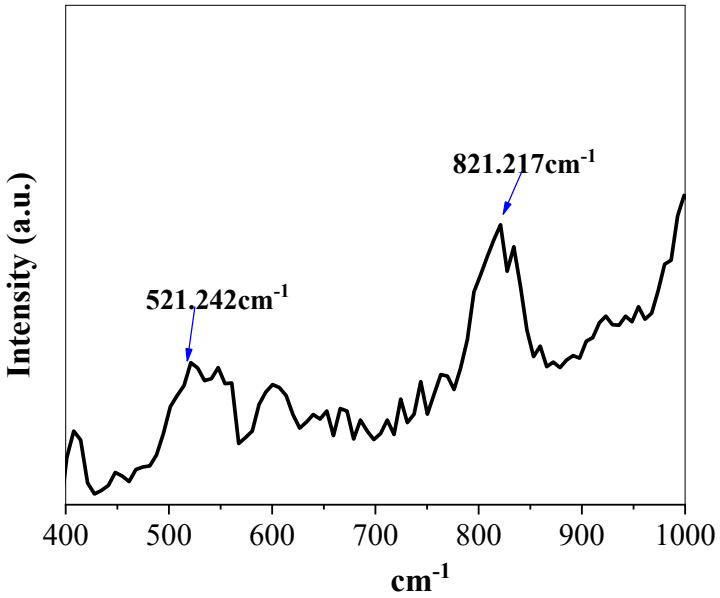

Fig. S8. Raman spectrum of $[Co(L)(\mu\text{-}OH)(\mu\text{-}OO)Co(L)]Cl_3$ **2**.

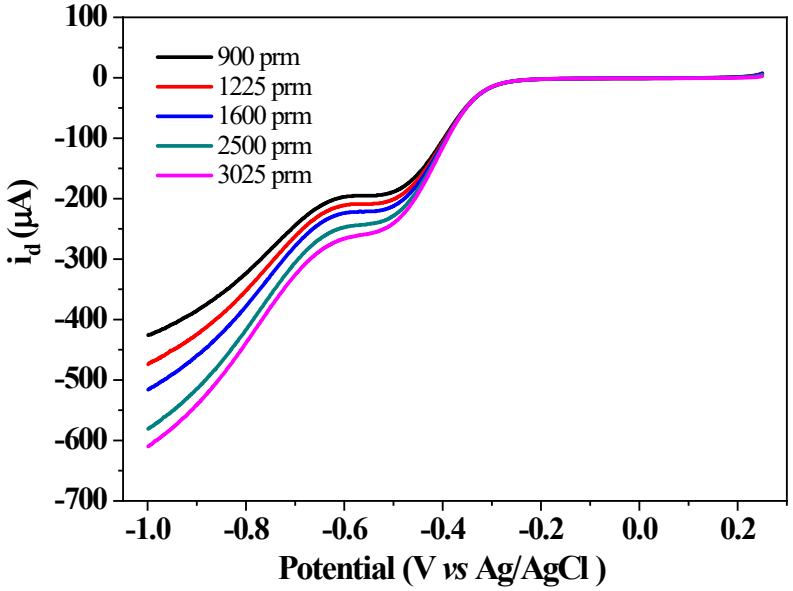

Fig. S9. Rotating ring-disk electrode (RRDE) measurement for O_2 reduction at the glassy carbon (GC) disk electrode loaded with $[Co(L)(Cl)_2]Cl$ **1** in an O_2-saturated 0.1 M KOH solution at various rotation rates. Conditions: work electrode, GC disk electrode; counter electrode, Pt ring electrode, 25 °C.

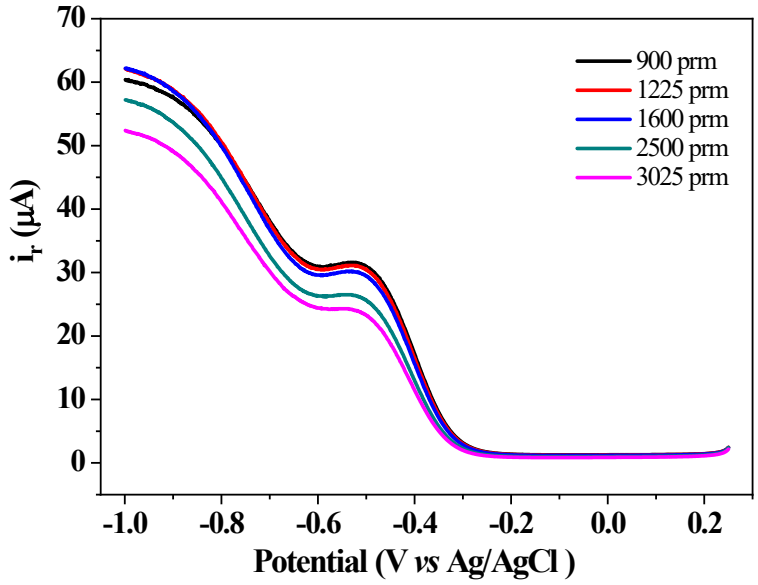

Fig. S10. RRDE measurement for O_2 reduction of the ring current loaded with $[Co(L)(Cl)_2]Cl$ **1** in an O_2-saturated 0.1 M KOH solution at various rotation rates. Conditions: work electrode, GC disk electrode; counter electrode, Pt ring electrode, 25 °C.

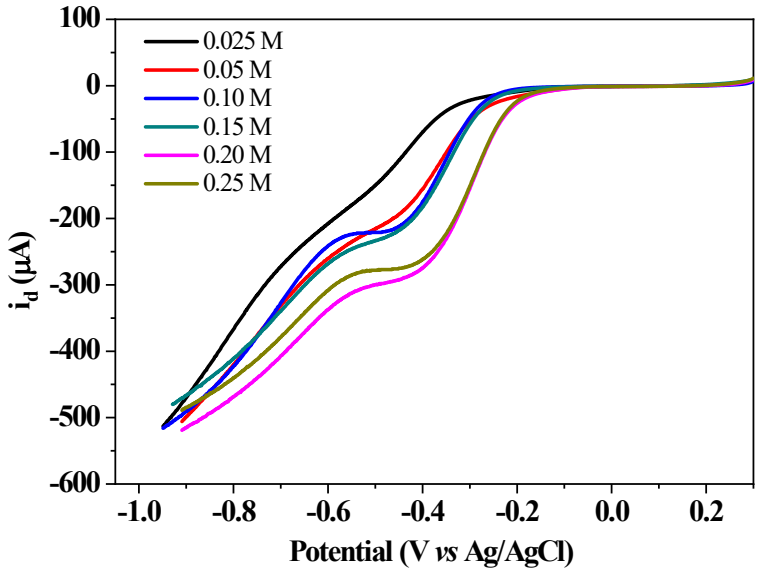

Fig. S11. RRDE measurement for O_2 reduction at the GC disk electrode loaded with $[Co(L)(Cl)_2]Cl$ **1** in an O_2-saturated with 1600 rpm at various KOH concentrations. Conditions: work electrode, GC disk electrode; counter electrode, Pt ring electrode, 25 °C.

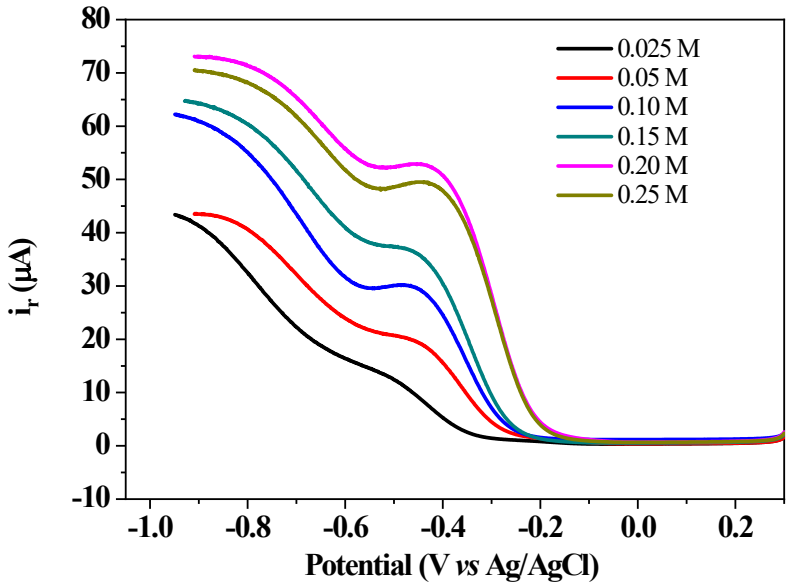

Fig. S12. RRDE measurement for O_2 reduction of the ring current loaded with $[Co(L)(Cl)_2]Cl$ **1** in an O_2-saturated with 1600 rpm at various KOH concentrations. Conditions: work electrode, GC disk electrode; counter electrode, Pt ring electrode, 25 °C.

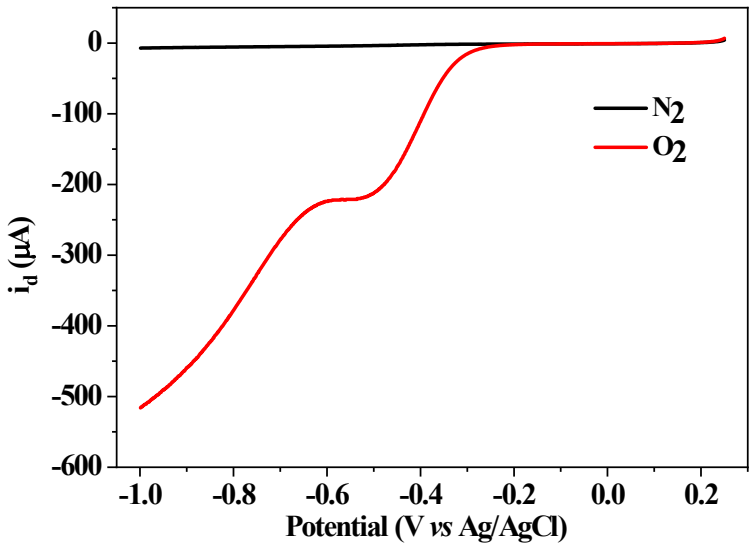

Fig. S13. RRDE measurement for O_2 reduction at the GC disk electrode loaded with $[Co(L)(Cl)_2]Cl$ **1** in a N_2-saturated and in an O_2-saturated 0.1 M KOH solution with 1600 rpm. Conditions: work electrode, GC disk electrode; counter electrode, Pt ring electrode, 25 °C.

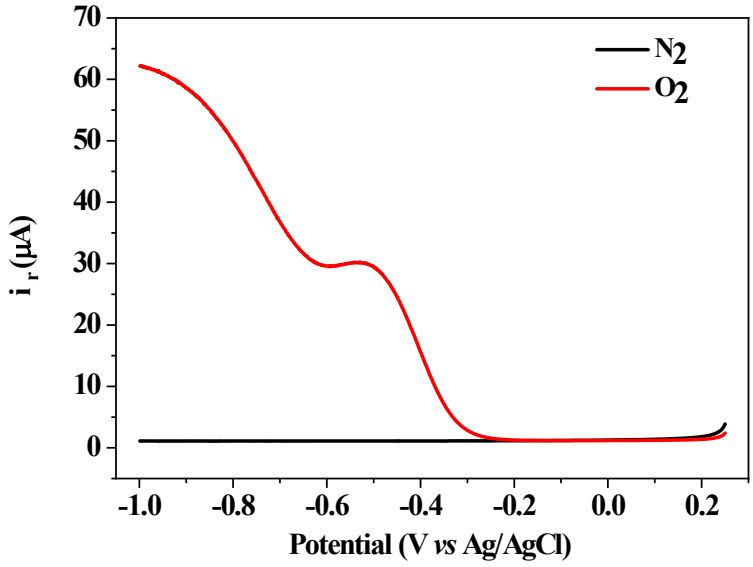

Fig. S14. RRDE measurement for O_2 reduction of the ring current loaded with $[Co(L)(Cl)_2]Cl$ **1** in a N_2-saturated and in an O_2-saturated 0.1 M KOH solution with 1600 rpm. Conditions: work electrode, GC disk electrode; counter electrode, Pt ring electrode, 25 °C.

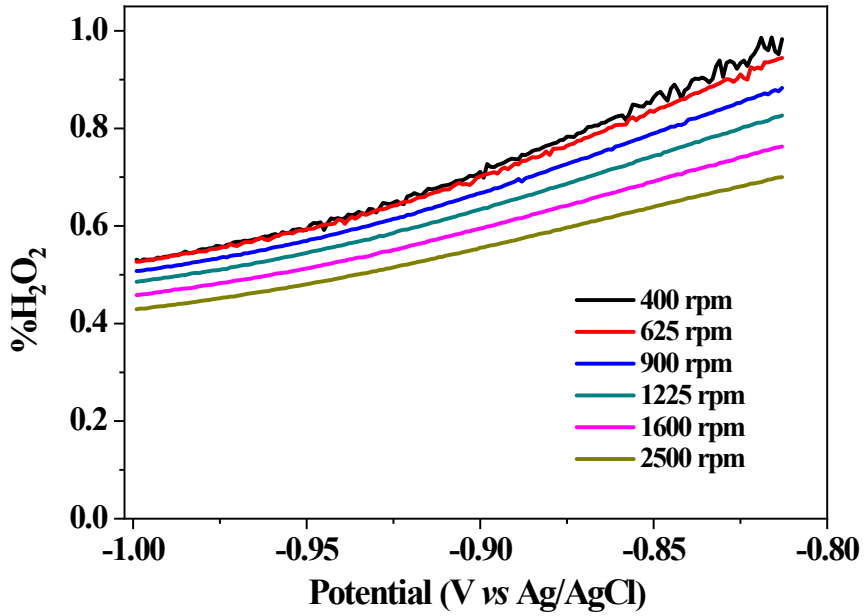

Fig. S15. The selectivity ($\%H_2O_2$) as a function of the disk potential with varying rotation rates, in 0.1 M KOH solution.

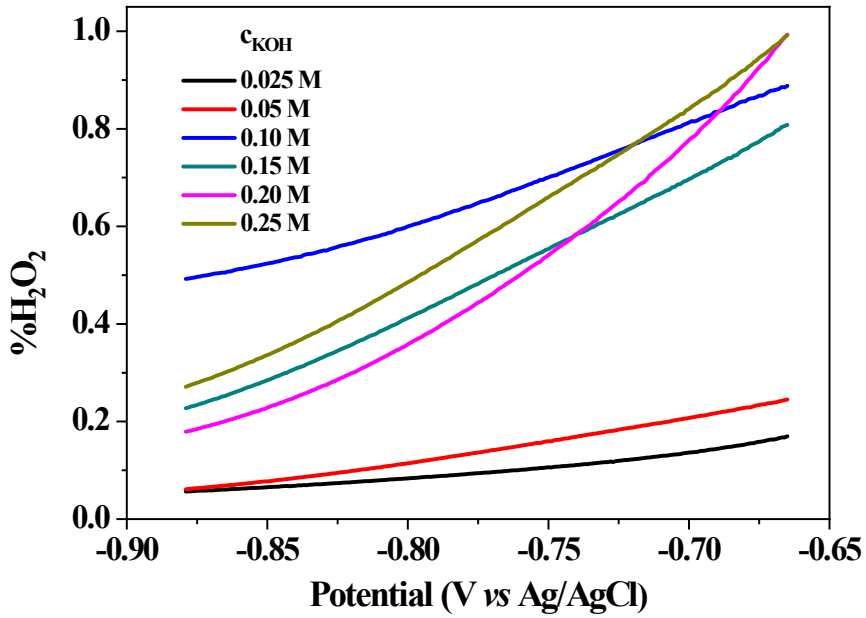

Fig. S16. The selectivity (%H_2O_2) as a function of the disk potential with different KOH concentrations at 1600 rpm.